Acousto-optic wavefront sensing and reconstruction

Adir Stup,[1,2] Eyal M. Cimet,[1,2] Erez N. Ribak,[1,*] and Vassilios Albanis[1,3]

[1]Department of Physics, Technion—Israel Institute of Technology, Haifa 32000, Israel

[2]Department of Electrical Engineering, Technion—Israel Institute of Technology, Haifa 32000, Israel

[3]Present address: Phase Focus, Ltd., Kroto Innovation Centre, University of Sheffield, Sheffield S3 7HQ, UK

*Corresponding author: eribak@physics.technion.ac.il

Received 21 April 2008; accepted 25 July 2008;
posted 29 July 2008 (Doc. ID 94992); published 20 August 2008

We employ an acousto-optic cell as a tunable-pitch wavefront sensor and study its performance. The index of refraction of two cross-standing waves forms, in the near field, an adjustable array of caustics. These caustics, similar to the lenslets used for Hartmann–Shack sensing, were measured to have an extended focal relief of 200 times their pitch. We discovered a strong interaction between the caustics and source speckle, so much so that we had to modulate the beam to reduce it. We measured ocular wavefronts at different frequencies and established the consistency and reliability of the reconstruction.

OCIS codes: 010.1080, 010.7350, 030.6140, 2230.1040.

1. Wavefront Sensing

The Hartmann–Shack (HS) wavefront sensor was developed to quantify permanent telescope aberrations and later to measure aberrations in the Earth's atmosphere in order to correct them [1]. Wavefront sensing and correction spread into other applications such as ocular optics or laser beam correction. Here we investigate an alternate form of HS sensing, employing wavefront sampling by acousto-optic caustics [2] instead of by holes or lenslets [3]. We demonstrate this flexible method by measurement of the human eye.

If the dimensions of the HS lenslets are negligible when compared to the cross section of the beam [1], we may analyze each lenslet as if a separate localized plane wave was incident to it. A near paraxial plane wave propagating at angles θ_x and θ_y in the x–z and y–z planes, respectively, can be described with spatial frequency components [4] $n\theta_x/\lambda_0$, $n\theta_y/\lambda_0$ (λ_0 is the wavelength and n is the refractive index), and the split plane waves are

$$u_D(x,y) = \sum_{k,l=1}^{N} u_{k,l}(x,y) \approx \sum_{k,l} A_{k,l} \times \exp\{-i\kappa[\theta_x^{k,l}(x - k\Delta) + \theta_y^{k,l}(y - l\Delta)]\}, \quad (1)$$

where Δ is the effective width of each lenslet, $k = 2\pi n/\lambda_0$ is the wavenumber, and we assume a Cartesian $N \times N$ lenslet array. $A_{i,j}$ is the average amplitude of $u(x,y)$ over the lenslet area $\Delta \times \Delta$. Propagating a distance F and reassembling the individual lenslet images [4], we obtain an overall output distribution known as a Hartmanngram:

$$H(x,y) \propto s(x,y) * \sum_{k,l} A_{k,l} \times \delta[x - (k\Delta + F\theta_x^{k,l}), y - (l\Delta + F\theta_y^{k,l})]. \quad (2)$$

We convolved the result with a finite diffraction spot [4] $s(x,y)$, resulting from the caustic shape of acoustic modulation, as shown below. When the whole wavefront is planar, we obtain a regular grid pattern (Fig. 1), which can serve as a reference. Given a Hartmanngram for an unknown wavefront, one may use the deviations from that reference and

0003-6935/09/0100A1-04$15.00/0

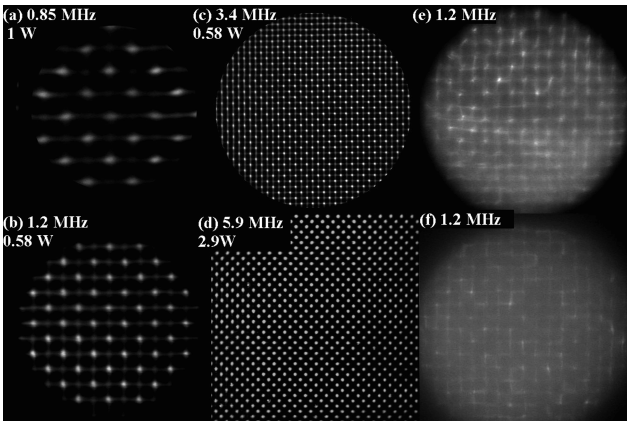

Fig. 1. (a)–(d) Reference images, white light: the power indicated is root-mean-square output, excluding returned power, which can be significant at resonance. (d) is magnified to show details. (e), (f) best ocular images, showing laser speckle–caustic interaction.

calculate the incident wavefront gradient to an accuracy dependent on the density of the lenslets. Methods for slope calculation include the classic centroid method [1,5] and the more robust Fourier demodulation [6].

2. Near-Field Caustics and Speckle

Acousto-optic diffraction is a photoelastic effect generated by a sound wave in an optical medium, which relates the periodic strain of the sound wave itself and the local compression to the refractive index [2]. This effect can be harnessed to implement various optical tasks, two of which we employ. The Raman–Nath regime, relevant here, may be described as a phase grating, allowing several far-field orders of diffraction at angles given by $\sin \varphi_m = \frac{1}{2}m\lambda/\Lambda$, where Λ, the acoustic wavelength, depends on f, the temporal frequency, and the speed of sound in the optical medium, here $c(\mathrm{H_2O}) \approx 1480\,\mathrm{ms^{-1}}$. Standing waves were chosen for their fixed positions in the acousto-optic cell (AOC), each having two nodes per cycle, so the optical pitch is halved [3],

$$\Lambda(f) = 2\pi/K(f) = c(\mathrm{H_2O})/f \equiv 2\Delta(f). \qquad (3)$$

The implementation of the AOC as a HS sensor is two-dimensional: two acoustic waves of the same frequency $\omega = 2\pi f$ in a given optical medium, propagating in two cross directions perpendicular to the optical axis. The index of refraction is related to the acoustic stress Δn [2,4]:

$$n(x,y,t) = n_0 - \Delta n[\cos(\omega t - Kx) + \cos(\omega t - Ky)].$$

As we tune the frequency, a standing wave is obtained, the profile becomes stationary, and the acousto-optic lenslet array is formed. The AOC may then be used in the *near field* as a HS sensor, with an effective focal length F determined by the acousto-optic properties and hitherto unmeasured. Hexagonal and cylindrical geometries [3] were also tested [7].

Speckles [8] resulting from scattering in the retina and the preceding inhomogeneous vitreous humor strongly affect ocular wavefront sensing, significantly more than in astronomy, and much more than in solid lenslet arrays, so much so that the method becomes invalid. This is related to the multiple speckle effect produced by random optical fields with two (or more) different correlation widths [9]. As a result of this effect, many HS spots either disappear or take a very elongated shape. Their images are not presentable, and we show only the very best in Figs. 1(e) and 1(f). This is an effect that received hitherto little attention, and we attribute it to the interaction of the random coherent field with the acoustically created optical near field. The interaction is much more severe compared to the solid lenslet arrays, possibly because of their shorter focal length (see below). This shorter propagation probably reduces the interaction with either the retinal or the vitreous humor speckle fields. To make the HS pattern visible again, we needed to employ another AOC in its far field to average the beams over space and time, resulting in a significant reduction of saturation and subsequent uniformity of the desired pattern [10].

3. Measuring Caustics

The experimental setup is designed with two purposes in mind: first, to measure the focal length of the acoustic caustics as a function of driving frequency and power; second, to obtain Hartmanngrams off a fast-varying and random-field target, represented by the live eye. The system may be grouped into three main units [Fig. 2(a)]. In order to obtain uniform Hartmanngrams at a controlled intensity, the laser source is sent through a polarizer as well as an antispeckle AOC [10]. A small fraction of the modulated beam is then split into the subject's eye and scattered out from the retina. This reflected beam then propagates through the HS imaging system: a telescopic lens pair magnifies the corneal image onto the main AOC (Fig. 2(b)), where the formed lenslet array focuses into a multitude of retinal images. A camera (lens and CCD detector) is shifted to have the array of foci focused on the detector. Adding a pinhole at the first retinal image was a practical method to rid the resulting images of unwanted reflections and to minimize HS spot size.

We determined the focal length of the AOC by first focusing the camera on the corneal image in the AOC center, then forming acoustically a lenslet array and focusing again to obtain the sharpest foci. The refocus gives us the lenslet focal length, $F(\omega) = d(\omega) - d(0)$, where $d(\omega)$ is the focus position at some frequency ω, to be compared to the focus without modulation ($\omega = 0$). We concentrated in the range $\omega \approx 0.5$–$10\,\mathrm{MHz}$, or equivalently lens pitch $\Delta \approx 1.5$–$0.07\,\mathrm{mm}$ [Eq. (3)], in resonance domains where little power is necessary, set by the piezoelectric transducer geometry (Fig. 1). The focal distance and shape as well as grid pattern are dependent on the resonance strength in the orthogonal directions, and to a lesser

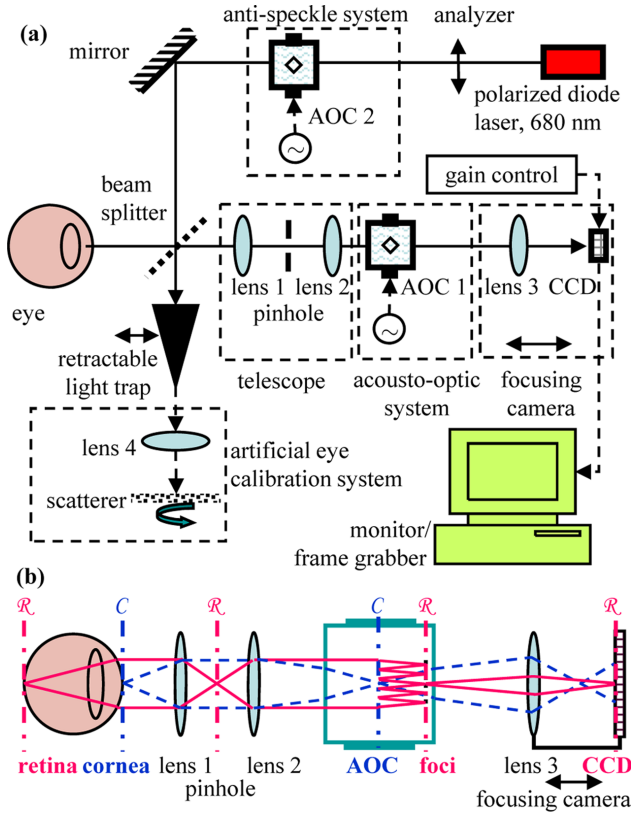

Fig. 2. (Color online) (a) An oscillating laser beam is scattered off the retina and reimaged by the acoustic wave into an array of retinal images to be imaged again by the camera. (b) Propagation of the two ocular planes: retinal (R) and corneal (C).

extent on the power driving the AOC: at low power, focusing is inefficient, and not far above that, nonlinearities deform the spot size but do not change the focal length significantly [11]. The rectangular dimensions of our AOC provide separate modes of vertical and horizontal resonance that are degenerate in a square cell. For example, in Fig. 1(a) the AOC is much more resonant vertically than horizontally. Another aspect is the grid regularity, which is dependent on the acoustic power setting, as well as occasional reflections from the walls, cell optical misalignment, or decentering. The Hartmanngrams display a secondary grid [Fig 1(b)], typical of periodic caustics [12]. A similar secondary grid also appears in solid lenslet arrays, which have a much shorter focal length. After considering spot size and shape as well as power consumption, the 3.2 MHz domain was found to be most effective: sampling density is conveniently 0.25 mm, and heating of the water caused by high power (leading to slow drift in frequency) is much weaker compared to the 5.9 MHz regime.

Figure 3 shows the long focal length of the lenslets in both white light and laser, growing as a function of their pitch. This important result proves that the AOC frequency response is independent of the coherence or spectral characteristics of the incident light. If any, chromatic differences are much smaller than the focal lengths themselves. Disperse data arise

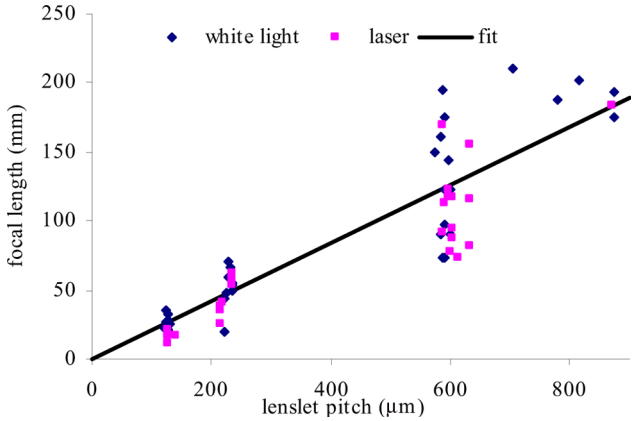

Fig. 3. (Color online) Focal length versus acoustic pitch. Scatter in the results is due to the large depth of focus of the caustics. The line fit is to $F[\text{mm}] = 0.21\Delta[\mu\text{m}] = 16/f[\text{MHz}]$.

from the difficulty in determining the focus location along the caustics, requiring its calibration, e.g., by a known aberration. A much weaker qualitative correlation was also found between the acoustic power and the lenslet power.

These results have consequences for astronomical adaptive optics [3]: for volume correction it is required to sense the wavefront at two or more consecutive planes, each conjugate to a different atmospheric turbulence layer. When applying the sensor in this mode, the lenslet foci of one layer-conjugate array fall on the same detector plane as the other layer array at alternating times [13]. For example, an array of 0.6 mm lenslets will be 100 mm before the detector, while a second array of 0.25 mm lenslets will be placed following it, 40 mm before the same detector (at the origin in Fig. 3). If the conjugate layers require very different sampling pitches from these, a relay lens might be inserted between the AOCs, still using the same detector.

4. Wavefront Reconstruction

We obtained ocular wavefronts of six consenting healthy subjects, ages 20–22, after dark adaptation. The amount of light never exceeded 45 μW, well below the damage threshold. References were taken immediately after measuring the eye itself, by exposing the reference calibration system, an artificial eye consisting of a lens and a rotating scatterer at its focus (Fig. 2). The data were preprocessed using high-pass filters and histogram equalization. A pupil-recognition algorithm was applied to the subject Hartmanngram, which in turn centered the desired image. In addition, it took a sample of the reference image in the same area, so that irregularities in the acoustic grid would be canceled. The final wavefront slope reconstruction and integration was then obtained using the Fourier demodulation [14,15]. The results in Figs. 4(c)–4(f) indicate near-sighted subjects, together with other aberrations such as astigmatism. Similar reconstructions at different frequencies and acquisition times are consistent to within a few percent.

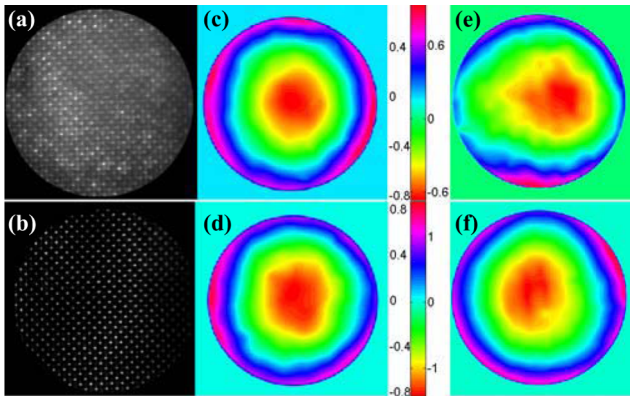

Fig. 4. (Color online) Hartmanngrams of (a) subject and (b) reference; (c) reconstruction, AOC frequency 3.543 MHz; (d) reconstruction of the same subject at 3.74 MHz; (e), (f) reconstructions from two more subjects at 3.2 MHz.

5. Conclusions

In summary, we measured the focal length of the acoustic caustics and were able to remove the attendant enhanced speckle. To our knowledge, this is the first focus measurement and the first related speckle smoothing for this device. The AOC has proved itself capable of wavefront sensing on the human eye with adjustable pitch and a very long focal length. Due to the dynamic nature of the system, calibration must be performed every so often. Future improvements of the system may include an automated device for simultaneous reference measurement.

Support for this work was provided by the EU Sharp-Eye and ELT networks and the French–Israeli Science Fund. We also thank our colleagues who agreed to take part in this experiment.

References

1. B. C. Platt and R. Shack, "History and principles of Shack–Hartmann wavefront sensing," J. Refract. Surg. **17**, 573–577 (2001).
2. A. Korpel, *Acousto-Optics* (CRC Press, 1997).
3. E. N. Ribak, "Harnessing caustics for wavefront sensing," Opt. Lett. **26**, 1834–1836 (2001).
4. B. E. A. Saleh and M. C. Teich, *Fundamental of Photonics* (Wiley, 1991).
5. P. M. Prieto, F. Vargas-Martín, S. Goelz, and P. Artal, "Analysis of the performance of the Hartmann–Shack sensor in the human eye," J. Opt. Soc. Am. A **17**, 1388–1398 (2000).
6. Y. Carmon and E. N. Ribak, "Phase retrieval by demodulation of a Hartmann-Shack sensor," Opt. Commun. **215**, 285–288 (2003).
7. I. Grulkowski and P. Kwiek, "Experimental study of light diffraction by standing ultrasonic wave with cylindrical symmetry," Opt. Commun. **267**, 14–19 (2006).
8. J. C. Dainty, ed., *Laser Speckle and Related Phenomena* (Springer, 1984).
9. I. Freund and D. A. Kessler, "Singularities in speckled speckle," Opt. Lett. **33**, 479–481 (2008).
10. V. Albanis, E. N. Ribak, and Y. Carmon, "Reduction of speckles in retinal reflection," Appl. Phys. Lett. **91**, 054104 (2007).
11. M. V. Berry and C. Upstill, "Catastrophe optics: morphologies of caustics and their diffraction patterns," in *Progress in Optics* E. Wolf, ed. (Elsevier, 1980), Vol. 18, pp. 257–346.
12. M. V. Berry, "Cusped rainbows and incoherence effects in the rippling-mirror model for particle scattering from surfaces," J. Phys. A **8**, 566–584 (1975).
13. A. Talmi and E. N. Ribak, "Direct demodulation of Hartmann–Shack patterns," J. Opt. Soc. Am. A **21**, 632–639 (2004).
14. Y. Carmon and E. N. Ribak, "Fast Fourier demodulation," Appl. Phys. Lett. **84**, 4656–4657 (2004).
15. E. N. Ribak, "Separating atmospheric layers in adaptive optics," Opt. Lett. **28**, 613–615 (2003).